

The Unusual Suppression of Superconducting Transition Temperature in Double-Doping 2H-NbSe₂

*Dong Yan¹, Yishi Lin², Guohua Wang³, Zhen Zhu³, Shu Wang¹, Lei Shi¹, Yuan He¹,
Man-Rong Li⁴, Hao Zheng³, Jie Ma³, Jinfeng Jia³, Yihua Wang², Huixia Luo^{1,5*}*

¹School of Material Science and Engineering, Sun Yat-Sen University, No. 135, Xingang Xi Road, Guangzhou, 510275, P. R. China

²Department of Physics, Fudan University, Shanghai, 200433, China

³Department of Physics and Astronomy, Shanghai Jiao Tong University, Shanghai 200240, China

⁴School of Chemistry, Sun Yat-Sen University, No. 135, Xingang Xi Road, Guangzhou, 510275, China

⁵Key Lab Polymer Composite & Functional Materials, Sun Yat-Sen University, No. 135, Xingang Xi Road, Guangzhou, 510275, P. R. China

E-mail: luohx7@mail.sysu.edu.cn

ABSTRACT

2H-NbSe₂ is one of the most widely researched transition metal dichalcogenide (TMD) superconductors, which undergoes charge-density wave (CDW) transition at T_{CDW} about 33 K and superconducting transition at T_c of 7.3 K. To explore the relation between its superconductivity and Fermi surface nesting, we combined S substitution with Cu intercalation in 2H-NbSe₂ to make Cu_xNbSe_{2-y}S_y ($0 \leq x = y \leq 0.1$). Upon systematic substitution of S and intercalation of Cu ions into 2H-NbSe₂, we found that when the Cu and S contents ($x = y \geq 0.06$) increases, the T_c decreases in Cu_xNbSe_{2-y}S_y. While at higher x and y values, T_c keeps a constant value near 2 K, which is not commonly observed for a layered TMD. For comparison, we found the simultaneous substitution of Nb by Cu and Se by S in Cu_xNb_{1-x}Se_{2-y}S_y ($0 \leq x = y \leq 0.06$) lowered the T_c substantially faster. We construct a superconducting phase diagrams for our double-doping compounds in contrast with the related single-ions doping systems.

KEYWORDS: Transition metal dichalcogenide, Cu_xNbSe_{2-y}S_y, Cu_xNb_{1-x}Se_{2-y}S_y, Superconductivity, Charge-density wave.

INTRODUCTION

Transition metal dichalcogenides (TMDs) with 1T (octahedrally coordinated) and 2H (trigonal prismatically coordinated) structures have attracted abundant research for decades due their various novel properties, *i. e.* superconductivity and charge density wave (CDW) and topological semimetal states.¹⁻⁸ 2H-NbSe₂ has been researched as the most famous layered superconducting TMD materials bearing CDW state with the superconducting transition temperature (T_c) of 7.3 K and a quasi-two-dimensional incommensurate CDW transition temperature (T_{ICDW}) of ~ 33 K.⁹ The co-existence of superconductivity and CDW state and its superconducting mechanism have made it a research hotspot.¹⁰⁻¹³ Even if 2H-NbSe₂ has been taken for representative superconductor for many years, it has also been recently found that 2H-NbSe₂ is a multiband superconductor with some similarities to that of MgB₂ superconductor.¹⁴⁻¹⁶ The relationship between its superconductivity and Fermi surface nesting is still under fierce debate.

In order to figure out this debate, numerous theoretical and experimental articles have been concentrated researching on its behavior. In the experimental case, researchers usually used the familiar and effective ways to tune the superconducting and CDW transition temperatures of this class, including chemical doping (*e.g.*, refs 17-22), adopting high pressure (*e.g.*, refs 23-26) and gating.²⁷ Especially, a large number of research papers focusing on tuning its superconducting and CDW behavior by chemical doping have been published. So far, all the inorganic doping 2H-NbSe₂ system shows lower T_c , comparing with the pristine 2H-NbSe₂. For example, the 3d transition metals such as Fe, Ni, Co, Zn, or Al have been used to intercalate into 2H-NbSe₂ and resulted in remarkable T_c drop.²⁸⁻²⁹ More recently, we studied the effect of Cu intercalation of 2H-NbSe₂ and found an unusual *S*-shaped superconducting phase diagram in 2H-Cu_xNbSe₂.²⁰ In most of the superconductors, the transition temperature T_c decreases with increasing disorder.³⁰ However, in the 2H-Cu_xNbSe₂ system, as is generally observed the T_c will drop off with an increased doping value when introduce “impurities” into an optimal superconductor, whereas the mode that T_c declined under such instance is novel: an *S*-shaped superconducting

phase diagram was obtained, near $x = 0.03$ with an inflection point and appearing a leveling off of the T_c about 3 K (usual value of layered TMD) at high doping content. In contrast, there is minor change in T_c of the S substitution for Se in 2H-NbSe₂ system.³¹⁻³²

Superconducting state coexists with a CDW state or occurs in proximity of such a state in most metallic TMDs. It has been thought for decades that the occurrence of a CDW state was associated with superconductivity. 2H-NbS₂ is isostructural and isoelectronic to 2H-NbSe₂ and with a T_c of 6.05 K, but no CDW order occurs,³³ which does not accord with the diversity of electronic instabilities in the TMDs. Pristine 2H-NbSe₂ and 2H-NbS₂ are both multiband superconductors, and the former one has a CDW state but the latter one doesn't.³³⁻³⁵ On the other hand, S doped 2H-NbSe₂ slightly affects the T_c but unusual S-shaped superconducting phase diagram is observed when Cu ions intercalated into 2H-NbSe₂.^{20, 31-32} 2H-NbSe₂ and 2H-NbS₂ thus open a door to the study of the interaction of CDW and multiband superconductivity phenomena in the bulk TMDs. Tuning the physical properties of CDW and superconducting states by chemical doping including substitution and intercalation is a common tool in the condensed matter field. In order to further study the interplay of the multiband superconductivity and CDW state in the TMDs, we proposed to combine with S substitution and Cu substitution/intercalation of 2H-NbSe₂. To the best of our knowledge, there was no work about double doping in 2H-NbSe₂ to date.

In this article we report the double doping Cu and S into 2H-NbSe₂ to form Cu_xNb_{1-x}Se_{2-y}S_y ($x = y = 0.06$) and Cu_xNbSe_{2-y}S_y ($0 \leq x = y \leq 0.1$), respectively, with remaining the 2H structure (see **Fig. 1A, B**). The material is multiple phases with $x > 0.1$ in Cu_xNbSe_{2-y}S_y and $x > 0.06$ in Cu_xNb_{1-x}Se_{2-y}S_y, and thus corresponding T_c cannot be reliably measured. Magnetic susceptibilities, resistivities, and heat capacities measurements were performed to characterize Cu_xNbSe_{2-y}S_y polycrystalline samples systematically. For comparison, magnetic susceptibilities of Cu_xNb_{1-x}Se_{2-y}S_y polycrystalline samples were also measured. The results signify that the T_c value has a diminution with increasing Cu and S content in both Cu_xNb_{1-x}Se_{2-y}S_y and

$\text{Cu}_x\text{NbSe}_{2-y}\text{S}_y$ case, which was usually observed when introduce “foreign matter” into the pristine 2H-NbSe₂ superconductors. However, we obtained an S-shaped superconducting phase diagram with T_c vs. x in the $\text{Cu}_x\text{NbSe}_{2-y}\text{S}_y$ case, having an inflexion at $x = 0.06$ and tending to smooth at high x value, from original T_c about 7.3 K in 2H-NbSe₂ to low T_c value near 2 K, which is similar to the single doping case Cu_xNbSe_2 . Besides, a half arc-shaped superconducting phase diagram with T_c vs. x was observed in the $\text{Cu}_x\text{Nb}_{1-x}\text{Se}_{2-y}\text{S}_y$ case. The superconducting state competes with CDW state in the layered $\text{Cu}_x\text{NbSe}_{2-y}\text{S}_y$ TMDs at low temperatures. The low-temperature scanning tunneling microscopy (STM) study reveals the formation of the 2×2 commensurate CDWs on the sample’s surface and with tiny variety in q vector of the charge density wave state arisen from the Cu intercalation and S substitution, weaken but not exterminate of the correlation of the CDW. The difference between other doped 2H-NbSe₂ materials such as $\text{NbSe}_{2-x}\text{S}_x$, Fe_xNbSe_2 , Cu_xNbSe_2 , and $\text{Cu}_x\text{Nb}_{1-x}\text{Se}_{2-y}\text{S}_y$ in the superconducting phase diagram revealed its uncommon character.

EXPERIMENTAL SECTION

$\text{Cu}_x\text{NbSe}_{2-y}\text{S}_y$ ($0 \leq x = y \leq 0.1$) and $\text{Cu}_x\text{Nb}_{1-x}\text{Se}_{2-y}\text{S}_y$ ($x = y = 0.06$) polycrystalline samples were synthesized *via* solid state method. Firstly, the mixture of reagent of Cu (99.9%), S (99.999%), Se (99.999%) and Nb (99.9%) in corresponding stoichiometric ratios were heated to 850 °C at a rate of 2 °C/min and held for 5 days in sealed vacuum silica glass tubes. Then the as-prepared polycrystalline samples were reground, re-pelletized, and sintered again *via* a rate of 5 °C/min to 850 °C and held for 2 days. The selected compositions single crystals were grown by the chemical vapor transport (CVT) method, using iodine as a transport agent. The $\text{Cu}_x\text{NbSe}_{2-y}\text{S}_y$ ($0 \leq x = y \leq 0.1$) as-prepared powders were mixed with iodine at quality ratio 20:1, then heated sealed vacuum silica tubes for 7 days in a two-zone furnace, where the growth and source zones temperatures were 625 and 725 °C, respectively. We also adopt the same method to synthesize the powder and single crystal sample of $\text{Cu}_x\text{Nb}_{1-x}\text{Se}_{2-y}\text{S}_y$ ($0 \leq x = y \leq 0.06$).

The morphologies of the single crystals were studied by scanning electron microscopy (SEM, Quanta 400F, Oxford) operated at 20 kV. The element distributions and element compositions of single crystals of $\text{Cu}_x\text{NbSe}_{2-y}\text{S}_y$ were investigated by energy dispersive X-ray spectroscopy (EDXS). The $\text{Cu}_{0.06}\text{NbSe}_{1.71}\text{S}_{0.08}$ sample was also characterized by a low-temperature STM (USM-1600, Unisoku) with an ultrahigh vacuum (base pressure $\sim 1 \times 10^{-10}$ torr) at $T = 4.8$ K. The sample was cleaved in situ at room temperature and then transferred into the STM head immediately. Electrochemically etched tungsten tips were used after heating and silver decoration.

We adopt powder X-ray diffraction (PXRD) with Bruker D8 Advance ECO equipping LYNXEYE-XE detector and Cu $K\alpha$ radiation to determine the phase purity of polycrystalline samples. The unit cell parameters were determined by profile fitting the powder diffraction data with the FULLPROF diffraction suite with Thompson-Cox-Hastings pseudo-Voigt peak shapes.³⁶ The temperature dependent electrical resistivity (4-point means), magnetic susceptibility and heat capacity of polycrystalline samples were measured by EverCool II Quantum Design Physical Property Measurement System (PPMS). The materials show no air-sensitivity sign in the period of measurements. T_{cS} were taken from the intersection of the extrapolations of the normal state and the steepest slope of the superconducting transition region susceptibility for magnetic susceptibility data; the midpoint of the resistivity transitions was referred from resistivities; meanwhile the T_{cS} obtained from the equal area construction method for heat capacity data.

RESULTS AND DISCUSSION

Figs. 1A-F show the unit cell parameters and PXRD pattern for $\text{Cu}_x\text{NbSe}_{2-y}\text{S}_y$ ($0 \leq x = y \leq 0.1$) and $\text{Cu}_x\text{Nb}_{1-x}\text{Se}_{2-y}\text{S}_y$ ($0 \leq x = y \leq 0.06$). The results show that the powder samples obtained was pure. The doping limit for substitution of S and intercalated Cu into 2H-NbSe_2 is $x = 0.1$. However, the limit for Cu and S co-substitution into 2H-NbSe_2 is $x = 0.06$. Impurities will appear as shown in Fig. 1A when the doping content over the limit. The unit cell parameters c for both $\text{Cu}_x\text{NbSe}_{2-y}\text{S}_y$ ($0 \leq x = y \leq$

0.1) and $\text{Cu}_x\text{Nb}_{1-x}\text{Se}_{2-y}\text{S}_y$ ($0 \leq x = y \leq 0.06$) increases linearly with increasing Cu and S content within the solid solution. c augments linearly from 12.5680(6) ($x = 0.00$) to 12.6166(3) ($x = 0.10$) in $\text{Cu}_x\text{NbSe}_{2-y}\text{S}_y$ and 12.5680(6) ($x = 0.00$) to 12.5853(3) ($x = 0.06$) in $\text{Cu}_x\text{Nb}_{1-x}\text{Se}_{2-y}\text{S}_y$, respectively, with Vegard's law type behavior. Inset of **Figs. 1A, B** show the position of peak (002) movement to left with more doping content. This also demonstrates that c will increase with augment of doping (**Fig. 1F**). **Figs. 1C, D** show the refinement results of powder 2H- $\text{Cu}_{0.04}\text{Nb}_{0.96}\text{Se}_{1.96}\text{S}_{0.04}$ and $\text{Cu}_{0.04}\text{NbSe}_{1.96}\text{S}_{0.04}$. These reflections can be indexed in $P6_3/mmc$ space group and the lattice parameters derived to be $a = 3.4480(3)$ Å and $c = 12.5785(9)$ Å for $\text{Cu}_{0.04}\text{Nb}_{0.96}\text{Se}_{1.96}\text{S}_{0.04}$, $a = 3.4457(3)$ Å and $c = 12.5859(9)$ Å for $\text{Cu}_{0.04}\text{NbSe}_{1.96}\text{S}_{0.04}$. The $\text{Cu}_x\text{NbSe}_{2-y}\text{S}_y$ crystal structure shows the central Nb in trigonal prismatic coordination by randomly occupied chalcogen (S and Se) to form MX_2 layer with Cu intercalating between these layers (**Fig. 1D**). The $\text{Cu}_x\text{Nb}_{1-x}\text{Se}_{2-y}\text{S}_y$ crystal structure shows the central Nb with Cu-doping in trigonal prismatic coordination by randomly occupied chalcogen (S and Se) to form MX_2 layer (**Fig. 1C**). **Figs. S1A-C** show the SEM and EDXS images of $\text{Cu}_{0.06}\text{NbSe}_{1.71}\text{S}_{0.08}$ single crystal. From **Fig. S1**, we can confirm that the composition of the single crystal is $\text{Cu}_{0.06}\text{NbSe}_{1.71}\text{S}_{0.08}$, which has a layer structure and will be used for scanning tunneling microscopy (STM) measurements later.

Figs. 2A, B show the temperature dependence of magnetic susceptibility under applied magnetic field of 20 Oe for $\text{Cu}_x\text{Nb}_{1-x}\text{Se}_{2-y}\text{S}_y$ ($0 \leq x = y \leq 0.06$) and $\text{Cu}_x\text{NbSe}_{2-y}\text{S}_y$ ($0 \leq x = y \leq 0.1$) in the temperature range 2 - 8 K, respectively. The measurements are performed under zero field cooling. **Fig. 2A** shows the rapid downtrend for $\text{Cu}_x\text{Nb}_{1-x}\text{Se}_{2-y}\text{S}_y$ ($0 \leq x = y \leq 0.06$), the T_c almost drops to 3.5 K when $x = 0.02$. As shown in **Fig. 2B**, in the case of $\text{Cu}_x\text{NbSe}_{2-y}\text{S}_y$ ($0 \leq x = y \leq 0.1$), T_c also decreases with the increase of the content of intercalation of Cu and substitution of S. We next adopt systematic research on $\text{Cu}_x\text{NbSe}_{2-y}\text{S}_y$. We further got the test on $\text{Cu}_x\text{NbSe}_{2-y}\text{S}_y$ polycrystalline samples after pelletized and sintered for temperature dependence of the normalized electrical resistivities ($\rho/\rho_{300\text{K}}$), as shown in **Fig. 2C**. We can easily find the obvious, sharp drop of $\rho(T)$ curves which represent the onset of

superconductivity at low temperatures (**Fig. 2D**). The T_c s declined with the increasing doping content. Also, this tendency is also apparently found by the susceptibility data of $\text{Cu}_x\text{NbSe}_{2-y}\text{S}_y$ (**Fig. 2B**) - the superconducting state moves to lower temperatures systematically with the increasing doping content in $\text{Cu}_x\text{NbSe}_{2-y}\text{S}_y$, which indicated by the negative magnetic susceptibility. The $\text{Cu}_x\text{NbSe}_{2-y}\text{S}_y$ samples show a metallic temperature dependence between 8 K to 300 K ($d\rho/dT > 0$). Also, at low temperature the $d\rho/dT$ vs. T curve shows peaks at the corresponding T_c s (inset of **Fig. 2C**).

In order to get more data of the superconductivity and electronic properties of $\text{Cu}_x\text{NbSe}_{2-y}\text{S}_y$ solid, we adopt heat capacity measurements on their polycrystalline samples. **Fig. 3** shows the temperature dependent zero-field heat capacity, that is C_p/T vs. T , for $\text{Cu}_{0.02}\text{NbSe}_{1.98}\text{S}_{0.02}$ sample. The heat capacity curve displays a sharp specific heat jump which indicates the superconducting transition temperature for this material. The obtained T_c from heat capacity is highly consistent with the T_c obtained by the $\chi(T)$ and $\rho(T)$ tests. The normal state of specific heat at high temperatures of zero magnetic field obey the relation of $C_p/T = \beta T^2 + \gamma$, where β and γ describe the phonon and electronic contributions to the heat capacity, respectively. We got the values of β and γ (inset of **Figs. 3**) from fitting the data obtained at 0 T field. The normalized specific heat jump value $\Delta C/\gamma T_c$ obtained from the data (**Figs. 3**) was 2.16 for $\text{Cu}_{0.02}\text{NbSe}_{1.98}\text{S}_{0.02}$ which was much higher than the Bardeen-Cooper-Schrieffer (BCS) weak-coupling limit value (1.43). Then we estimate the Debye temperature by the formula $\Theta_D = (12\pi^4 n R / 5\beta)^{1/3}$ by using the fitted value of β , where R is the gas constant and n is the number of atoms per formula unit. The lattice becomes more stable when the Se-Se Van der Waals bonds were changed into Se-Cu-Se ionic bonds by increasing Cu content in $\text{Cu}_x\text{NbSe}_{2-y}\text{S}_y$ which reflected in the result **Figs. 3** shows that the Debye temperature increase modestly (Table 1). Thus, we can calculate the electron-phonon coupling constant (λ_{ep}) by using the Debye temperature (Θ_D) and critical temperature T_c from the inverted McMillan formula:³⁷ $\lambda_{ep} = \frac{1.04 + \mu^* \ln\left(\frac{\Theta_D}{1.45 T_c}\right)}{(1 - 1.62 \mu^*) \ln\left(\frac{\Theta_D}{1.45 T_c}\right) - 1.04}$ the values of λ_{ep} are 0.80 for $\text{Cu}_{0.02}\text{NbSe}_{1.98}\text{S}_{0.02}$ (**Table 1**). This value suggests strong coupling superconductivity properties. The electron density of states at the Fermi

level ($N(E_F)$) can be calculated from $N(E_F) = \frac{3}{\pi^2 k_B^3 (1 + \lambda_{ep})} \gamma$ with the γ and λ_{ep} . This yields value that $N(E_F) = 4.08$ states/eV f.u. for NbSe₂ and $N(E_F) = 3.62$ states/eV f.u. for Cu_{0.02}NbSe_{1.98}S_{0.02} (**Table 1**). The results indicate that the density of electronic states at the Fermi energy thus decreases obviously with increasing Cu content into 2H-NbSe₂. With the goal of determining the critical fields $\mu_0 H_{c2}(0)$, we further examined temperature dependent electrical resistivity under applied magnetic for selected Cu_xNbSe_{2-y}S_y samples. **Fig. 4** reveals the $\rho(T, H)$ data measured for Cu_xNbSe_{2-y}S_y ($x = 0.01, 0.02$) which was shown as an example. The inset of **Figs. 4A and B** show upper critical field values $\mu_0 H_{c2}$ plotted vs. temperature with T_c s obtained from resistively different applied fields. The solid lines through the data show the nicely linear fitting for $\mu_0 H_{c2}$ vs. T curve near T_c of two selected samples. The value of fit data slopes (dH_{c2}/dT) of selected samples are shown in **Table 1**. We can estimate the zero-temperature upper critical fields (upper inset of **Figs. 4A and B**) to 3.5 T for Cu_{0.01}NbSe_{1.99}S_{0.01} and 3.0 T for Cu_{0.02}NbSe_{1.98}S_{0.02} from these data, using the Werthamer-Helfand-Hohenberg (WHH) expression for the dirty limit superconductivity, $\mu_0 H_{c2} = -0.693 T_c (dH_{c2}/dT_c)$.³⁷⁻⁴¹ Also the results obtained were summarized in **Table 1**. The Pauli limiting field for Cu_xNbSe_{2-y}S_y ($x = 0.01, 0.02$) was calculated from $\mu_0 H^P = 1.86 T_c$. The calculated values of $\mu_0 H^P$ were larger than the estimated values. Then, with this formula $\mu_0 H_{c2} = \frac{\phi_0}{2\pi \xi_{GL}^2}$, where ϕ_0 is the flux quantum, the Ginzburg-Laudau coherence length ($\xi_{GL}(0)$) was calculated ~ 9.7 nm for Cu_{0.01}NbSe_{1.99}S_{0.01}, and ~ 10.3 nm for Cu_{0.02}NbSe_{1.98}S_{0.02} (**Table 1**).

STM imaging gives rise to the real space electronic state information, which has been proved to be the direct experimental evidence of a CDW phases. The Cu_{0.06}NbSe_{1.71}S_{0.08} sample was characterized by our low-temperature STM. **Fig. 5** presents the STM image, which clearly displays the formation of the 2×2 commensurate CDW on the sample's surface. (The voltage dependent STM images are shown in SI **Figure S1**). We thus confirmed the formation of CDW on the sample.

Finally, we got the superconductivity phase diagram plotted T_c s vs doping content for 2H-Cu_xNbSe_{2-y}S_y ($0 \leq x = y \leq 0.1$) was summarized in **Fig. 6**. As

comparison, the information for Cu_xNbSe_2 , Fe_xNbSe_2 and $\text{NbSe}_{2-x}\text{S}_x$ ($0 \leq x \leq 0.1$) were all taken from those previous literatures. The T_c s extracted from the resistivity measurements performed here for $\text{Cu}_x\text{NbSe}_{2-y}\text{S}_y$; the x dependence of T_c . It's not surprising that the T_c of sulfur doped material of 2H-NbSe₂ presents a very small change compared to the T_c of pure NbS₂ (2H structure) of 6.5 K. In contrast, intercalation of magnetic ions may lead to a sharp drop of T_c , so that the T_c s decrease very rapidly with increasing Fe content in Fe_xNbSe_2 . However, nonmagnetic chemically Cu intercalation was found to act somewhere between the Fe- and S-doped extremes in T_c vs x curves, with a previously unknown example of an S-shaped suppression of T_c by substitution or doping in a single-phase material. This phenomenon also exists in Cu- and S-doping of 2H-NbSe₂ ($\text{Cu}_x\text{Nb}_{1-x}\text{Se}_{2-y}\text{S}_y$). Thus, when we adopt Cu-intercalation and S-substitution in 2H-NbSe₂ simultaneously, the T_c decrease light rapidly and the leveling off appear at lager x content compared with Cu_xNbSe_2 . $\text{Cu}_x\text{NbSe}_{2-y}\text{S}_y$ materials may provide a new platform for our understanding of multiband superconductivity phenomena and CDW in TMDs

Acknowledgements

H. X. Luo acknowledges the financial support by “Hundred Talents Program” of the Sun Yat-Sen University and Natural Science Foundation of China (21701197). H. Zheng, J. Ma, Y.H. Wang are supported by the “One Thousand Youth Talents” Program of China. M.R. Li is supported by the he “One Thousand Youth Talents” Program and the National Natural Science Fund of China (NSFC-21875287). H. Zheng is supported by the National Natural Science Foundation of China (Grant No. 11674226, 1790313); National Key Research and Development Program of China (Grant No. 2016YFA0300403). J. Ma is supported by the National Natural Science Foundation of China (Grant No. 11774223). We are grateful to Weiwei Xie for fruitful discussions.

References

- [1] Lee H N S, McKinzie H, Tannhauser, D S, and Wold A 1969 The low-temperature transport properties of NbSe₂. *J. Appl. Phys.* **40** 602-4.
- [2] Yang J J, Choi Y J, Oh Y S, Hogan A, Horibe Y, Kim K, Min B I and Cheong S W 2012 Charge-Orbital Density Wave and Superconductivity in the Strong Spin-Orbit Coupled IrTe₂:Pd. *Phys. Rev. Lett.* **108** 116402.
- [3] Rossnagel K 2011 On the origin of charge-density waves in select layered transition-metal dichalcogenides. *J. Phys.: Condens. Matter.* **23** 213001.
- [4] Gamble F R, Osiecki J H, Cais M and Pisharody R 1971 Intercalation complexes of lewis bases and layered sulfides: a large class of new superconductors. *Science* **174** 493-7.
- [5] Belopolski I, Xu S, Ishida Y, Pan X, Yu P, Sanchez D S, Zheng H, Neupane M, Alidoust N, Chang G, Chang T, Wu Y, Bian G, Huang S, Lee C, Mou D, Huang L, Song Y, Wang B, Wang G, Yeh Y, Yao N, Rault J E, Fevre P L, Bertran F, Jeng H, Kondo T, Kaminski A, Lin H, Liu Z, Song F, Shin S and Hasan M Z 2016 Fermi arc electronic structure and Chern numbers in the type-II Weyl semimetal candidate Mo_xW_{1-x}Te₂. *Phys. Rev. B* **94** 085127.
- [6] Belopolski I, Sanchez D S, Ishida Y, Pan X, Yu P, Xu S, Chang G, Chang T, Zheng H, Alidoust N, Bian G, Neupane M, Huang S, Lee C, Song Y, Bu H, Wang G, Li S, Eda G, Jeng H, Kondo T, Lin H, Liu Z, Song F, Shin S and Hasan M Z 2016 Discovery of a new type of topological Weyl fermion semimetal state in Mo_xW_{1-x}Te₂. *Nat. Commun.* **7** 13643.
- [7] Zheng H, Xu S, Bian G, Guo C, Chang G, Sanchez D S, Belopolski I, Lee C, Huang S, Zhang X, Sankar R, Alidoust N, Chang T, Wu F, Neupert T, Chou F, Jeng H, Yao N, Bansil A, Jia S, Lin H and Hasan M Z 2016 Atomic-Scale Visualization of Quantum Interference on a Weyl Semimetal Surface by Scanning Tunneling Microscopy. *ACS Nano* **10** 1378-85.
- [8] Fei F, Bo X, Wang R, Wu B, Jiang J, Fu D, Gao M, Zheng H, Chen Y, Wang X, Bu H, Song F, Wan X, Wang B and Wang G 2017 Nontrivial Berry phase and type-II Dirac transport in the layered material PdTe₂. *Phys. Rev. B* **96** 041201(R).
- [9] Revolinsky E, Lautenschlager E P and Armitage C H 1963 Layer structure superconductor. *Solid State Commun.* **1** 59-61.
- [10] Smaalen S V 2005 The Peierls transition in low-dimensional electronic crystals. *Acta. Cryst.* **A61** 51-61.
- [11] Wang H T, Li L J, Ye D S, Cheng X H and Xu Z A 2007 Effect of Te doping on superconductivity and charge-density wave in dichalcogenides 2H-NbSe_{2-x}Te_x (x = 0, 0.1, 0.2). *Chin. Phys. Soc.* **16** 2471-4.
- [12] Yokoya T, Kiss T, Chainani A, Shin S, Nohara M and Takagi H 2001 Fermi surface sheet-dependent superconductivity in 2H-NbSe₂. *Science* **294** 2518-20.
- [13] Gabovich A M, Voitenko A I and Ausloos M 2002 Charge- and spin-density waves in existing superconductors: competition between Cooper pairing and Peierls or excitonic instabilities. *Phys.Rep.* **367** 583-709.

- [14] Tsuei C C and Kirtley J R 2002 *d*-Wave pairing symmetry in cuprate superconductors-fundamental implications and potential applications. *Physica C: Superconductivity* **367** 1-8.
- [15] Souma S, Machida Y, Sato T, Takahashi T, Matsui H, Wang S C, Ding H, Kaminski A, Campuzano J C, Sasaki S and Kadowaki K 2003 The origin of multiple superconducting gaps in MgB₂. *Nature* **423** 65-7.
- [16] Örda T and Kristoffe N 2002 Modeling MgB₂ two-gap superconductivity. *Physica C: Superconductivity* **370** 17-20.
- [17] Fang L, Zou P Y, Wang Y, Tang L, Xu Z, Chen D H, Shan C L and Wen H H 2005 Competition of superconductivity and charge density wave order in Na_xTaS₂ single crystals. *Sci. Technol. Adv. Mater.* **6** 736-9.
- [18] Wagner K E, Morosan E, Hor Y S, Tao J, Zhu Y, Sanders T, McQueen T M, Zandbergen H W, Williams A J, West D V and Cava R J 2008 Tuning the Charge Density Wave and Superconductivity in Cu_xTaS₂. *Phys. Rev. B* **78** 104520.
- [19] Morosan E, Zandbergen H W, Dennis B S, Bos J W G, Onose Y, Klimczuk T, Ramirez A P, Ong N P and Cava R J 2006 Superconductivity in Cu_xTiSe₂. *Nat. Phys.* **2** 544-50.
- [20] Luo H X, Strychalska-Nowak J, Li J, Tao J, Klimczuk T and Cava R J 2017 S-Shaped Suppression of the Superconducting Transition Temperature in Cu-Intercalated NbSe₂. *Chem. Mater.* **29** 3704-12.
- [21] Luo H X, Xie W W, Tao J, Inoue H, Gyenis A, Krizan J W, Yazdani A, Zhu Y M and Cava R J 2015 Polytypism, polymorphism, and superconductivity in TaSe_{2-x}Te_x. *Proc. Natl. Acad. Sci.* **112** E1174-80.
- [22] Sugawara K, Yokota K, Takei N, Tanokura Y and Sekine T 1994 Three-dimensional collective flux pinning in the layered superconductor 2H-NbSe_{2-x}S_x. *J. Low Temp. Phys.* **95** 645-62.
- [23] Kusmartseva A F, Sipos B, Berger H, Forró L and Tutiš E 2009 Pressure Induced Superconductivity in Pristine 1T-TiSe₂. *Phys. Rev. Lett.* **103** 236401-4.
- [24] Joe Y I, Chen X M, Ghaemi P, Finkelstein K D, de la Pena G A, Gan Y, Lee J C T, Yuan S, Geck J, MacDougall G J, Chiang T C, Cooper S L, Fradkin E and Abbamonte P 2014 Emergence of charge density wave domain walls above the superconducting dome in 1T-TiSe₂. *Nat. Phys.* **10** 421-5.
- [25] Sipos B, Kusmartseva A F, Akrap A, Berger H, Forró L and Tutiš E 2008 From Mott state to superconductivity in 1T-TaS₂. *Nat. Mater.* **7** 960-5.
- [26] Singh Y, Nirmala R, Ramakrishnan S and Malik S K 2005 Competition between superconductivity and charge-density-wave ordering in the Lu₅Ir₄(Si_{1-x}Ge_x)₁₀ alloy system. *Phys. Rev. B* **72** 045106-13.
- [27] Ye J T, Zhang Y J, Akashi R, Bahramy M S, Arita R and Iwasa Y 2012 Superconducting Dome in a Gate-Tuned Band Insulator. *Science* **338** 1193-6.
- [28] Hauser J J, Robbins M and DiSalvo F J 1973 Effect of 3d impurities on the superconducting transition temperature of the layered compound NbSe₂. *Phys. Rev. B* **8** 1038-42.

- [29] Voorhoeve-Van Den Berg J M 1972 On the ternary phases Al_xNbSe_2 and Cu_xNbSe_2 . *J. Less-Common. Metals.* **26** 399-402.
- [30] Anderson P W, 1959, The theory of dirty of superconductors. *J. Phys. Chem. Solids*, **11**, 26-30.
- [31] Sugawara K, Yokota K, Tanokura Y, Sekine T, 1993 Anisotropy of flux flow in layered superconductor $2\text{H-NbSe}_{2-x}\text{S}_x$. *J. Low Temp. Phys.* **90** 305.
- [32] Sugawara K, Yokota K, Takei N, Tanokura Y, Sekine T, 1994 Dimension of the collective pinning in the layered superconductor $2\text{H-NbSe}_{2-x}\text{S}_x$, *Physica B* **194-196** 1891-1892
- [33] Naito M, Tanaka S, 1982 Electrical Transport Properties in 2H-NbS_2 , $-\text{NbSe}_2$, $-\text{TaS}_2$ and $-\text{TaSe}_2$. *J. Phys. Soc. Jpn.* **51**, 219-227.
- [34] Guillamo I, Suderow H, Vieira S, Cario L, Diener P, Rodiere P, 2008 Superconducting Density of States and Vortex Cores of 2H-NbS_2 . *Phys. Rev. Lett.* **101**, 166407.
- [35] Kačmarčík J, Pribulová Z, Marcenat C, Kleinc T, Rodič P, Cario L, Samuely P, 2010 Studies on two-gap superconductivity in 2H-NbS_2 . *Phys. C* **470** 719-720.
- [36] Rodríguez-Carvajal J 2001 Recent developments of the program FULLPROF. *Comm. Powder Diffr.* **26** 12-19.
- [37] McMillan W L 1968 Transition temperature of strong-coupled superconductors. *Phys. Rev.* **167** 331.
- [38] Wilson J A, Barker A S, Salvo Di F J and Ditzemberger J A 1978 Infrared properties of the semimetal TiSe_2 . *Phys. Rev. B* **18** 2866-75.
- [39] Kohn W 1967 Excitonic Phases. *Phys. Rev. Lett.* **19** 439-42.
- [40] Werthamer N R, Helfand E and Hohenberg P C 1967 Temperature and Purity Dependence of the Superconducting Critical Field H_{c2} . IV. Strong-Coupling Effects. *Phys. Rev.* **147** 415-6.
- [41] Kresin V Z and Wolf S A 1990 Fundamentals of superconductivity, Plenum Press, New York and London 150-153. .

Table 1. Characterization of the superconductivity in the $\text{Cu}_x\text{NbSe}_{2-y}\text{S}_y$ family.

$x = y$ in $\text{Cu}_x\text{NbSe}_{2-y}\text{S}_y$	0	0.01	0.02	0.04	0.05	0.06	0.07	0.08	0.09
T_c (K)	7.16	6.78	6.12	4.65	3.93	3.77	2.91	2.34	2.26
γ ($\text{mJ mol}^{-1} \text{K}^{-2}$)	17.4(20)	-	15.31(5)		-		-	-	-
β ($\text{mJ mol}^{-1} \text{K}^{-4}$)	0.56	-	0.55		-		-		-
Θ_D (K)	218(16)	-	220(2)		--		-	-	-
$\Delta C/T_c$	2.04	-	2.16		-		-	-	-
λ_{ep}	0.81	-	0.80		-			-	-
$N(E_F)$ (states/eV f.u)	4.08	-	3.62		-		-	-	-
$-dH_{c2}/dT$ (T/K)	1.95(4)	0.735 (2)	0.713 (5)	-	-		-	-	-
$\mu_0 H_{c2}$ (T)	9.7(2)	3.5(3)	3.0(2)	-	-		-	-	-
$\mu_0 H^P$ (T)	13.2	12.6	11.3	8.6	7.3	7.0	5.4	4.3	4.2
$\xi_{GL}(0)$ (nm)	5.8	9.7	10.3	-	-		-	-	-

Figures legends

Figure 1. Structural and chemical characterization of $\text{Cu}_x\text{Nb}_{1-x}\text{Se}_{2-y}\text{S}_y$ and $\text{Cu}_x\text{NbSe}_{2-y}\text{S}_y$. (A) Powder XRD patterns (Cu $K\alpha$) for the $\text{Cu}_x\text{Nb}_{1-x}\text{Se}_{2-y}\text{S}_y$ samples studied ($0 \leq x \leq 0.1$). Inset shows the enlargement of peak (002). (B) Powder XRD patterns (Cu $K\alpha$) for the $\text{Cu}_x\text{NbSe}_{2-y}\text{S}_y$ samples studied ($0 \leq x \leq 0.1$). Inset shows the enlargement of peak (002). (C) Powder XRD pattern with Rietveld refinement for $\text{Cu}_{0.04}\text{Nb}_{0.96}\text{Se}_{1.96}\text{S}_{0.04}$. Inset shows the crystal structure of 2H-NbSe₂ with Cu- and S-doping. (D) Powder XRD pattern with Rietveld refinement for $\text{Cu}_{0.04}\text{NbSe}_{1.96}\text{S}_{0.04}$. Inset shows the crystal structure of 2H-NbSe₂ with Cu-intercalation and S-doping. (E) The evolution of lattice parameter a of $\text{Cu}_x\text{NbSe}_{2-y}\text{S}_y$ and $\text{Cu}_x\text{Nb}_{1-x}\text{Se}_{2-y}\text{S}_y$. (F) The evolution of lattice parameter c of $\text{Cu}_x\text{NbSe}_{2-y}\text{S}_y$ and $\text{Cu}_x\text{Nb}_{1-x}\text{Se}_{2-y}\text{S}_y$.

Figure 2. Transport characterization of the normal states and superconducting transitions for $\text{Cu}_x\text{NbSe}_{2-y}\text{S}_y$ and $\text{Cu}_x\text{Nb}_{1-x}\text{Se}_{2-y}\text{S}_y$. (A) Magnetic susceptibilities for $\text{Cu}_x\text{NbSe}_{2-y}\text{S}_y$ ($0 \leq x = y \leq 0.06$) at the superconducting transitions; applied DC fields are 20 Oe. (B) Magnetic susceptibilities for $\text{Cu}_x\text{NbSe}_{2-y}\text{S}_y$ ($0 \leq x = y \leq 0.1$) at the superconducting transitions; applied DC fields are 20 Oe. (C, D) The temperature dependence of the resistivity ratio ($\rho/\rho_{300\text{K}}$) for polycrystalline $\text{Cu}_x\text{NbSe}_{2-y}\text{S}_y$ ($0 \leq x = y \leq 0.1$). Inset of (C) shows metallic temperature dependence ($d\rho/dT$) in the temperature region of 2 - 8 K.

Figure 3. Heat Capacity characterization of $\text{Cu}_{0.02}\text{NbSe}_{1.98}\text{S}_{0.02}$. Debye temperature of $\text{Cu}_{0.02}\text{NbSe}_{1.98}\text{S}_{0.02}$ obtained from fits to data in applied field. Inset show heat capacities through the superconducting transitions without applied magnetic field for $\text{Cu}_{0.02}\text{NbSe}_{1.98}\text{S}_{0.02}$.

Figure 4. Characterization of the critical fields of $\text{Cu}_x\text{NbSe}_{2-y}\text{S}_y$. (A, B): Low temperature resistivity at various applied fields for the examples of $\text{Cu}_{0.01}\text{NbSe}_{1.99}\text{S}_{0.01}$ and $\text{Cu}_{0.02}\text{NbSe}_{1.98}\text{S}_{0.02}$

Figure 5. A STM image ($15 \times 15\text{nm}^2$, 0.1V, 2nA) and its corresponding Fourier transformed image on a $\text{Cu}_{0.06}\text{NbSe}_{1.71}\text{S}_{0.08}$ surface. Both the patterns in real space and reciprocal space clear show the appearance of the 2×2 charge density waves. In the Fourier transformed image, the red (black) circle marks the one-fold (two -fold) lattice.

Figure 6. The superconducting phase diagram for 2H- $\text{Cu}_x\text{NbSe}_{2-y}\text{S}_y$ and 2H- $\text{Cu}_x\text{Nb}_{1-x}\text{Se}_{2-y}\text{S}_y$ compared to those of 2H- Cu_xNbSe_2 , 2H- $\text{NbSe}_{2-x}\text{S}_x$, and 2H- Fe_xNbSe_2 (Refs.16, 24, 28).

Fig. 1.

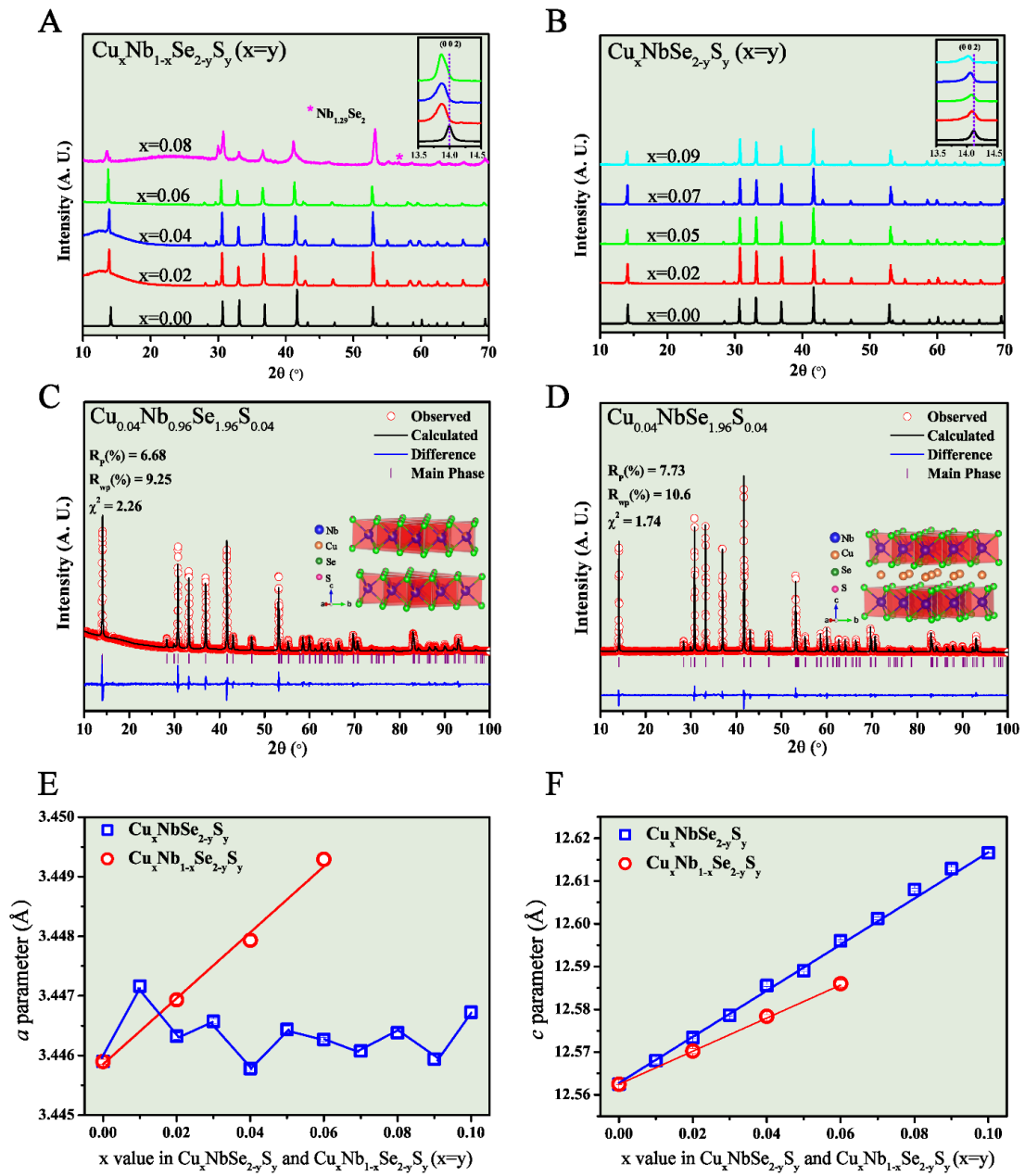


Fig. 2.

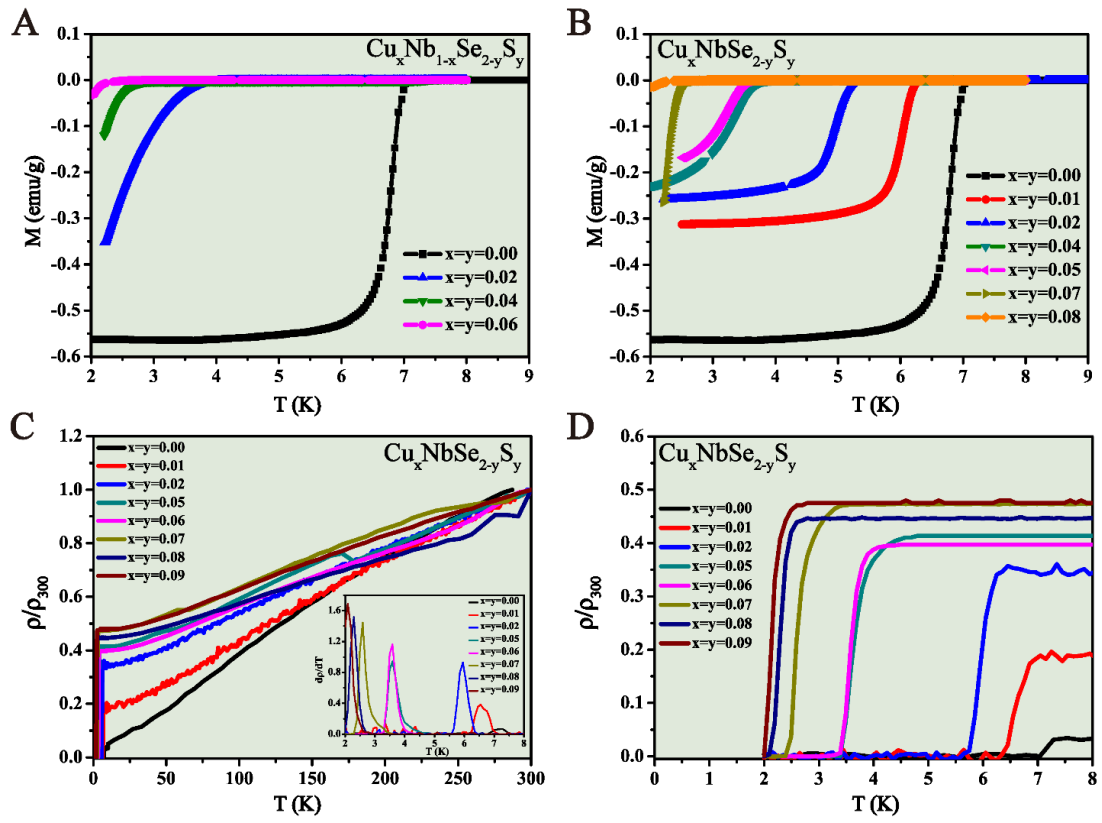


Fig. 3.

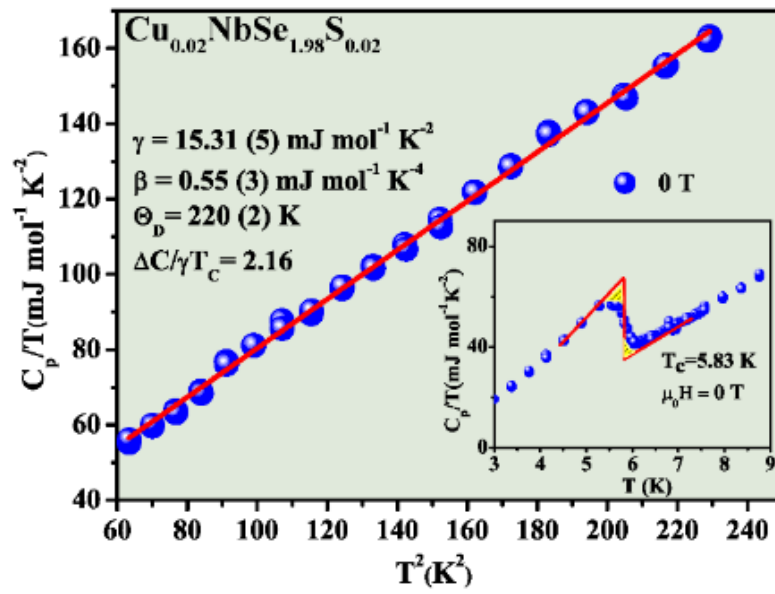


Fig. 4.

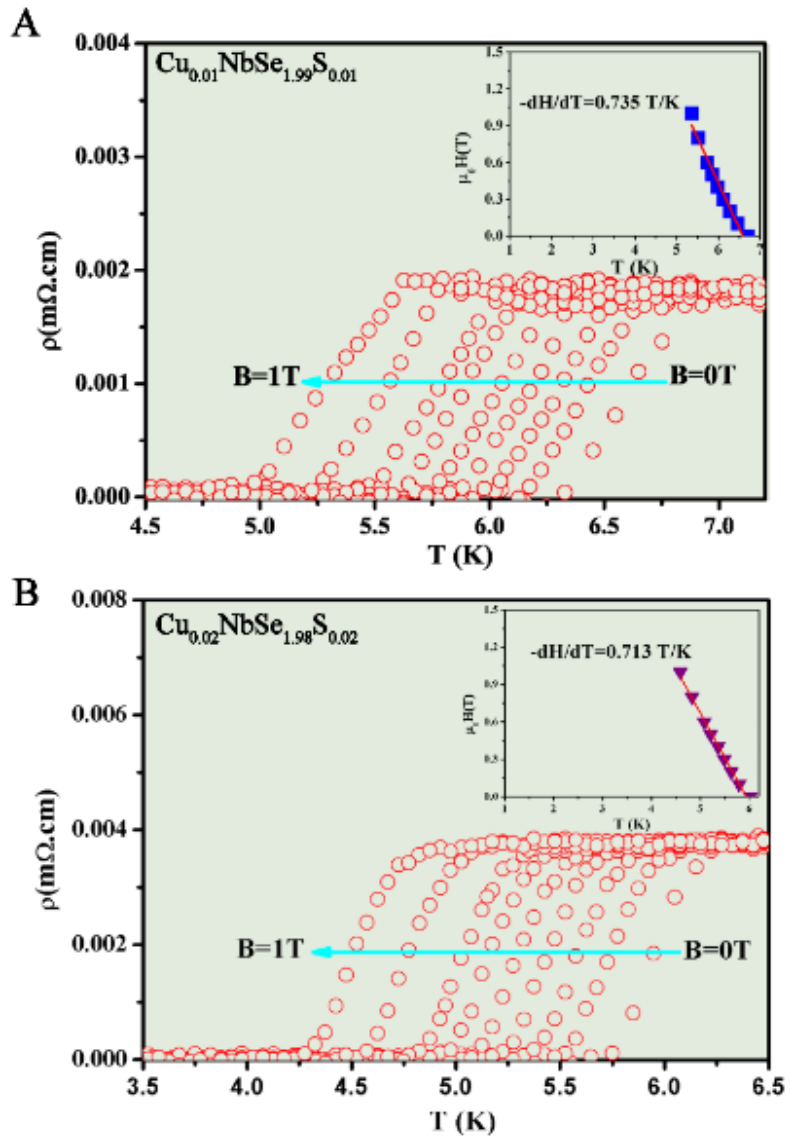


Fig. 5.

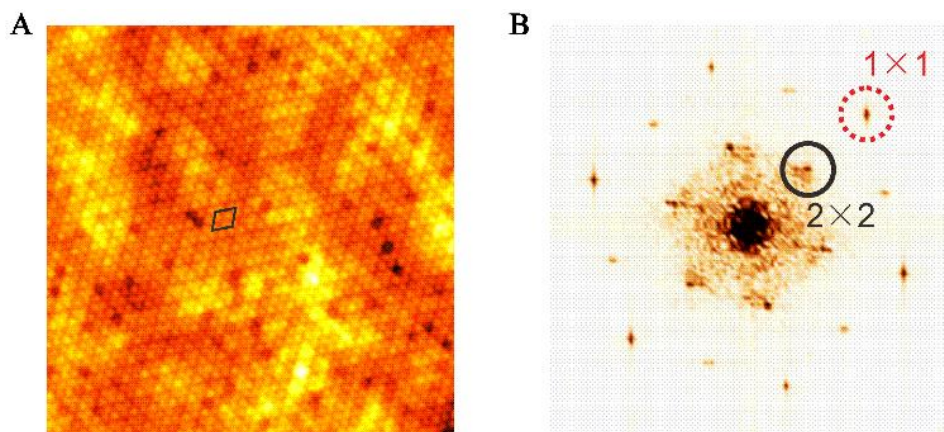
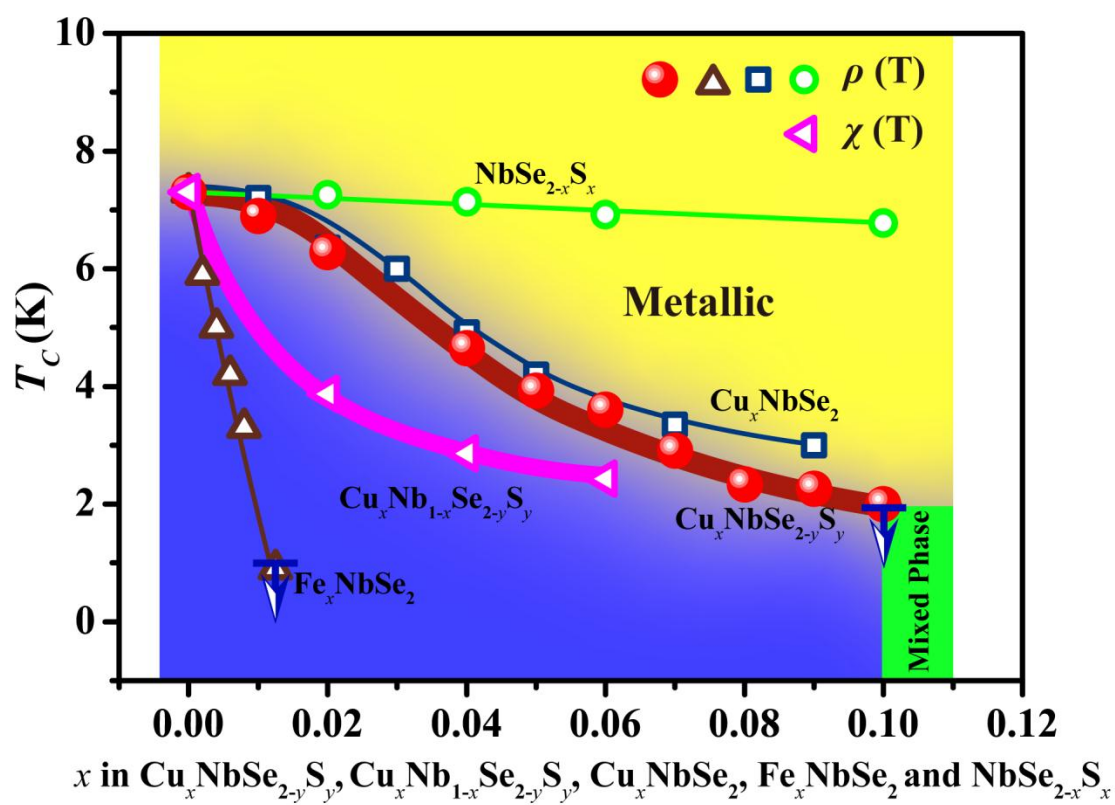


Fig. 6.



The Unusual Suppression of Superconducting Transition Temperature in Double-Doping 2H-NbSe₂

*Dong Yan¹, Yishi Lin², Guohua Wang³, Zhen Zhu³, Shu Wang¹, Lei Shi¹, Yuan He¹,
Man-Rong Li⁴, Hao Zheng³, Jie Ma³, Jinfeng Jia³, Yihua Wang², Huixia Luo^{1*}*

¹School of Material Science and Engineering and Key Lab Polymer Composite & Functional Materials, Sun Yat-Sen University, No. 135, Xingang Xi Road, Guangzhou, 510275, P. R. China

²Department of Physics, Fudan University, Shanghai, 200433, China

³School of Physics and Astronomy, Shanghai Jiao Tong University, Shanghai 200240, China

⁴School of Chemistry, Sun Yat-Sen University, No. 135, Xingang Xi Road, Guangzhou, 510275, China

E-mail: luohx7@mail.sysu.edu.cn

Supporting Information

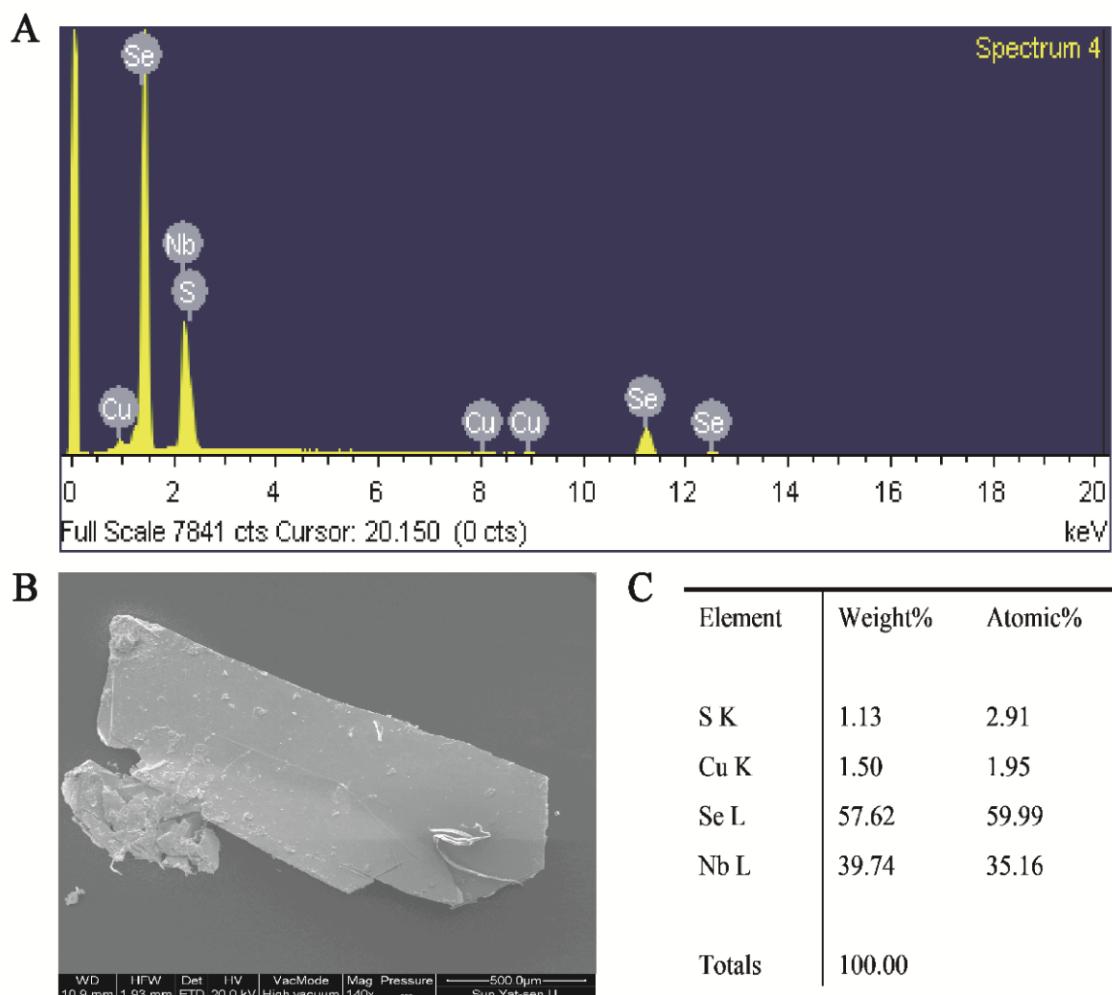


Figure S1. SEM and EDXS tests on the single crystals of $\text{Cu}_x\text{NbSe}_{2-y}\text{S}_y$. (A) EDXS spectrum of $\text{Cu}_{0.06}\text{NbSe}_{1.71}\text{S}_{0.08}$. (B) SEM image of $\text{Cu}_{0.06}\text{NbSe}_{1.71}\text{S}_{0.08}$ in the magnification of 140. (C) Element ratio of $\text{Cu}_{0.06}\text{NbSe}_{1.71}\text{S}_{0.08}$.

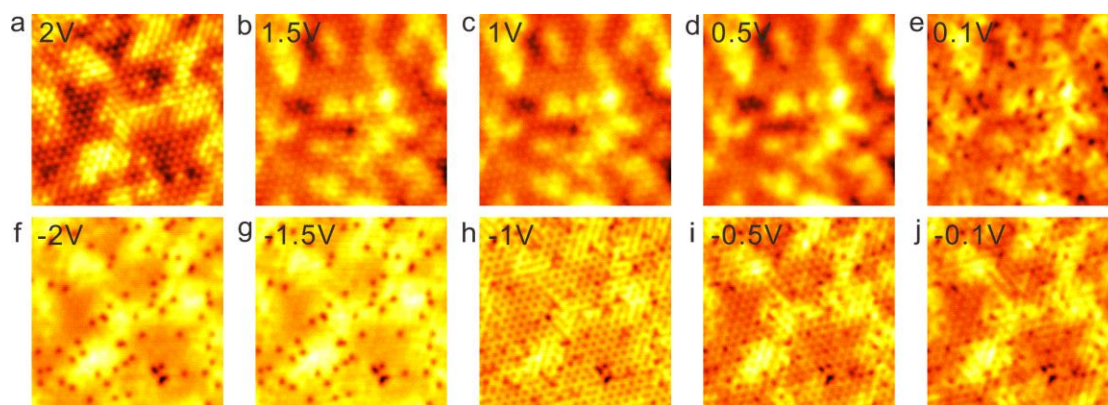


Figure S2. The voltage dependent STM images (all sizes of $15 \times 15 \text{ nm}^2$) on a $\text{Cu}_{0.06}\text{NbSe}_{1.71}\text{S}_{0.08}$ surface. Voltages are indicated on the figures. Tunneling current is 1 nA (a-c, f-j) and 0.1 nA (d and e), respectively. Panel a, f-j are measured on same area, while b-e are acquired on another area.